

Research Article

Chrysin Inhibits Indonesian Serotype Foot-and-Mouth-Disease Virus Replication: Insights from DFT, Molecular Docking, and Molecular Dynamics Analyses

Agus Susilo^{1*}, Miftakhul Cahyati², Nurjannah³, Dodyk Pranowo⁴, Feri Eko Hermanto⁵, Elma Putri Primandasari⁶

1)Department of Animal Products Technology, Faculty of Animal Science, Universitas Brawijaya, Malang 65145, Indonesia

2)Department of Oral Medicine, Faculty of Dentistry, Universitas Brawijaya, Malang 65145, Indonesia

3)Department of Statistics, Faculty of Mathematics and Natural Sciences, Universitas Brawijaya, Malang 65145, Indonesia

4)Department of Agro-industrial Technology, Faculty of Agricultural Technology, Universitas Brawijaya, Malang 65145, Indonesia

5)Faculty of Animal Sciences, Universitas Brawijaya, Malang 65145, Indonesia

6)Department of Business and Hospitality, Faculty of Vocational, Universitas Brawijaya, Malang 65145, Indonesia

* Corresponding author, email: agussusilo@ub.ac.id

Keywords:

3C Protease
antivirus

Chrysin

Foot-and-Mouth-Disease Virus

Propolis.

Submitted:

15 March 2023

Accepted:

23 August 2023

Published:

08 January 2024

Editor:

Furzani Binti Pa'ee

ABSTRACT

Chrysin, a predominant compound in Propolis, possesses diverse bioactivities, including antiviral properties. However, its antiviral efficacy against the Indonesian Foot-and-Mouth Disease Virus (FMDV) serotype remains unexplored. This study investigates Chrysin's inhibitory potential against FMDV Indonesian serotype by targeting the 3C Protease (3CP), a vital enzyme for viral replication. Multiple sequence alignment was used to reveal unique characteristics of the Indonesian serotype's 3CP compared to global serotypes. Density Functional Theory (DFT) calculations assessed Chrysin's interaction with 3CP based on electronegativity features. Molecular docking and molecular dynamics analyses evaluated Chrysin's inhibitory activity against 3CP, using homology modeling for the Indonesian serotype's 3CP structure. Luteolin, a known FMDV 3CP inhibitor with a similar structure to Chrysin, served as a reference. Results showed distinct 3CP sequences in the Indonesian serotype compared to O serotypes and others. Chrysin exhibited potential electron-donor activity with lower HOMO and LUMO values than Luteolin, but they had similar energy gaps, i.e., 4.016 and 4.044 eV, respectively. Molecular docking indicated similar binding affinities, with Chrysin (-6.365 kcal/mol) and Luteolin (-6.864 kcal/mol) bound to active site residues. Molecular dynamics analysis demonstrated stable 3CP-Chrysin and 3CP-Luteolin complexes, with minor differences in Radius of gyration (Rg) and Root-Mean-Square Fluctuation (RMSF) below 1 Å. From the ligand stability point of view, Chrysin had comparable stability with Luteolin. However, Chrysin formed fewer hydrogen bonds and displayed greater free-binding energy than Luteolin during simulation periods. These findings suggest that Chrysin holds promise as an inhibitor of the Indonesian serotype's FMDV 3C Protease.

Copyright: © 2024, J. Tropical Biodiversity Biotechnology (CC BY-SA 4.0)

INTRODUCTION

The recent Foot-and-Mouth-Disease (FMD) outbreak in Indonesia has struck cattle farming in Indonesia. The outbreak affected 20 provinces, which

was first reported in East Java province before it had widespread across the Indonesian archipelago. Although no zoonotic case was reported, the outbreak has affected human welfare by attacking economic values since livestock is categorized as a valuable asset in the community (IFRC 2022). As acute and systemic domestic animal diseases, FMD was caused by FMD Virus (FMDV) infection. Seven serotypes have been identified: A, O, C, Asia1, and South African Territories (SAT) serotypes SAT1, SAT2, and SAT3 (Grubman & Baxt 2004), and Indonesian serotype is classified as serotype O (Carrillo et al. 2005). The genetic diversity of FMDV, as represented by various serotypes, impacts both its antigenicity and viral structure, thereby hindering effective control through cross-protection measures, including vaccination (Li et al. 2021; Tesfaye et al. 2022). Hence, a promising approach to control FMDV involves targeting the non-structural proteins of the virus (Curry et al. 2007), as most vaccines primarily target structural proteins (typically inactivated or live-attenuated forms) (Kamel et al. 2019).

Non-structural proteins are typically enzymes that play a role in the assembly of viral structures (Han et al. 2015). Upon infection, FMDV will quickly transcribe and translate its genome to construct both structural and non-structural proteins, then produces a new virus particle (Wang et al. 2015). Those processes are mainly orchestrated by 3 Cysteine Protease (3CP), a non-structural protein and also an enzyme that catalyzes the cleaving of immature proteins into mature viral particles (Wang et al. 2015). Most drugs have been developed targeting this enzyme due to its essential activity in increasing viral load (Curry et al. 2007; Roqué Rosell et al. 2014). Besides, some natural products like Luteolin, Isoginkgetin, Andrographolide, and Deoxyandrographolide have also been evaluated to have antiviral activity through inhibition of 3CP of FMDV serotype A (Theerawatanasirikul et al. 2021; Theerawatanasirikul et al. 2022). Nevertheless, there is no information on the inhibitory activity against 3CP from the Indonesian serotype, since Indonesian serotype was classified into serotype O (Carrillo et al. 2005). Still, there is an opportunity for natural products to be involved in the development of controlling FMDV infection.

Propolis, also known as bee glue, is one of the products from bee farms. It is collected by bee workers from various plants' resinous secretion and mixed with a salivary and enzymatic substance to produce a wax-like substance (Anjum et al. 2019). Beyond the plant resins and essential oils, propolis also contains several bioactive molecules ranging from polyphenols to several minerals (Trusheva et al. 2011; Anjum et al. 2019). Due to its rich active compound, propolis has been widely used as an active pharmaceutical ingredient with countless biological activities (Rosyidi et al. 2018; Šuran et al. 2021; Zuhendri et al. 2021; Hidayat et al. 2022) Among several bioactive molecules in propolis, Chrysin constitutes the largest compounds (Wang et al. 2015). A previous study reported that Chrysin could inhibit the activity of 3CP of Enterovirus 71 and Coxsackievirus B3 as the primary infectious agent in Hand-Foot-and-Mouth Disease (HFMD) (Wang et al. 2014; Song et al. 2015). However, there is no information regarding the activity of Chrysin against the 3CP of FMDV.

Density functional theory (DFT) is a widely used computational method in chemistry and materials science to calculate the electronic structure of molecules and solids. One of the applications of DFT is in mapping the electronegativity of ligands prior to the molecular docking process (Yele et al. 2021). Electronegativity quantifies an atom's ability to attract electrons to itself in a chemical bond. The objective of molecu-

lar docking is to predict the binding affinity between a ligand and a protein. As it influences the distribution of electrons in the ligand and the protein, the electronegativity of a ligand may influence its binding affinity to a protein (Palko et al. 2021). Employing quantum mechanical method to predict the electronegativity, as DFT does, would be useful in improving binding affinity estimations (Ryde & Söderhjelm 2016). Moreover, the DFT technique also produced a geometry- optimized and energy -minimized structure (Bálint & Jäntschi 2021), which helps to reach the optimum molecular docking analysis (Ramírez-Velásquez et al. 2022). Therefore, by combining the DFT technique, molecular docking, and molecular dynamics approach, this study will explore the potential activity of Chrysin as the inhibitor of 3CP of FMDV, particularly for Indonesian serotype.

MATERIALS AND METHODS

Alignment of 3CP of FMDV serotypes

Amino acid sequences of several 3CPs from available FMDV serotypes were retrieved from GenBank database. The detailed identities of selected sequences as mentioned in the supplementary file table S1. Sequence alignment was performed in BioEdit software (Hall 1999) with the default parameters.

Protein Modeling and Binding Site Determination

The 3D structure of 3CP was homology-modeled by SwissModel (Waterhouse et al. 2018) according to the sequence obtained from the GenBank protein database with accession number AAT01756.1 (Carrillo et al. 2005). The structure of 3CP from FMDV serotype A10 (Protein Data Bank Identity, PDB ID: 2WV5) was used as the template. The active site residues were selected according to the previous elucidated structure, i.e., 2WV5 (Zunszain et al. 2010). Those active site then selected to guide the molecular docking step.

Ligand Structure Retrieval

Chrysin' and Luteolin's Three-dimensional (3D) structure was retrieved from the PubChem database (Kim et al. 2023) with compound identity (CID) 5281607 and 5280445, respectively. The isomeric Simplified Molecular-Input Line-Entry System (SMILES) was used for geometry optimization in the subsequent analysis.

Geometry Optimization and Density-Functional Theory Calculation

The 3D of Chrysin and Luteolin was built by Avogadro 1.2.0 software (Hanwell et al. 2012) according to the SMILES code. The geometry optimization was performed by ORCA 5.0.3 (Neese et al. 2020). The input for ORCA software was generated by Avogadro extension with B3LYP hybrid functional and def2-SVP basis set (Weigend & Ahlrichs 2005; Siiskonen & Priimagi 2017) settings. The Density Functional Theory (DFT) calculation output was analyzed and visualized using Avogadro to study the electronegativity properties of Chrysin and Luteolin. This involved representing the Highest Occupied Molecular Orbital (HOMO) and Lowest Unoccupied Molecular Orbital (LUMO) as blue for atoms with positive energy and red for atoms with negative energy. In addition, the value of the energy gap (ΔE) was calculated by the following equation (Rammohan et al. 2020; Maqsood et al. 2022):

$$\Delta E = E_{\text{LUMO}} - E_{\text{HOMO}} \quad (1)$$

Also, ionization potential (IP) and electron affinity (EA) were also determined according to the Hartree-Fock (HF) model with the following

equations (Rammohan et al. 2020; Hossen et al. 2021):

$$IP = -E_{\text{HOMO}} \quad (2)$$

$$EA = -E_{\text{LUMO}} \quad (3)$$

Molecular Docking

AutoDock Vina version 1.2.3 was employed to do molecular docking in a PyRx packages (Trott & Olson 2010; Dallakyan & Olson 2015; Eberhardt et al. 2021) according to the previous workflow (Hermanto et al. 2019). The 3D structure of Chrysin was inserted into PyRx software by OpenBable software (O'Boyle et al. 2011). The structure was energy-minimized using a universal force-field (uff) before the docking process. The docking was performed by setting 3CP and Chrysin as macromolecule and ligand, respectively. The docking will provide the ligand's binding energy and the binding pose. The structural interaction between 3CP and Chrysin was analyzed by Discovery Studio 2019 and visualized by PyMOL.

Molecular Dynamics and Free Binding Energy Calculation

YASARA 20.12.24 was employed to perform the molecular dynamics analysis (Krieger & Vriend 2015). The system was set as the previous study (Hermanto et al. 2022): pH 7.4; 0.9% NaCl concentration; 0.997 water density; 1 atm pressure, and 310°K temperature, cubic grid shape, 50 ns simulation time under AMBER14 forcefield (Maier et al. 2015). The structural dynamics were presented as the Root-Mean-Square Deviation (RMSD) of atom position or Root-Mean-Square Fluctuation (RMSF) of the residue's atoms. Furthermore, the free binding energy is also calculated according to the Molecular Mechanics – Poisson-Boltzmann Surface Area (MM-PBSA) (Homeyer & Gohlke 2012) equation in YASARA binding energy macros.

RESULTS AND DISCUSSION

Amino Acid Mutation of 3CP of Indonesian Serotypes Compared to Other Variants

The amino acid sequences alignment revealed slight variations in the arrangement of amino acids among Indonesian serotypes compared to other serotypes, excluding SAT serotypes. In particular, significant differences were observed at positions T104 and D177 among O serotypes, with most O serotypes having amino acids V and E. Notably, the sequences of the 3CP of Indonesian serotypes were distinct from other O serotypes, suggesting a unique structure for the 3CP of Indonesian serotypes. However, there were no mutations in the active site residues of Indonesian serotypes when compared to all the analysed serotypes (see supplementary file figure S1).

Structural Stability of 3CP of Indonesian Serotypes

Since the amino acid sequences of 3CP of Indonesian serotypes were different compared to the other O serotypes, the structural instability may happen. In addition, there is no available crystallographic structure of Indonesian serotypes in the database. Therefore, homology modelling was performed to obtain the 3D structure of 3CP of Indonesian serotypes. Upon modelling, the structure was then evaluated for its stability using molecular dynamics analysis compared to the available experimental structure of 3CP protein, i.e., 2WV5.

The modelling process resulted in a highly similar structure to the template, with both structures having a root mean square deviation (RMSD) of less than 1 Å (see figure 1A). The structural stability, as indi-

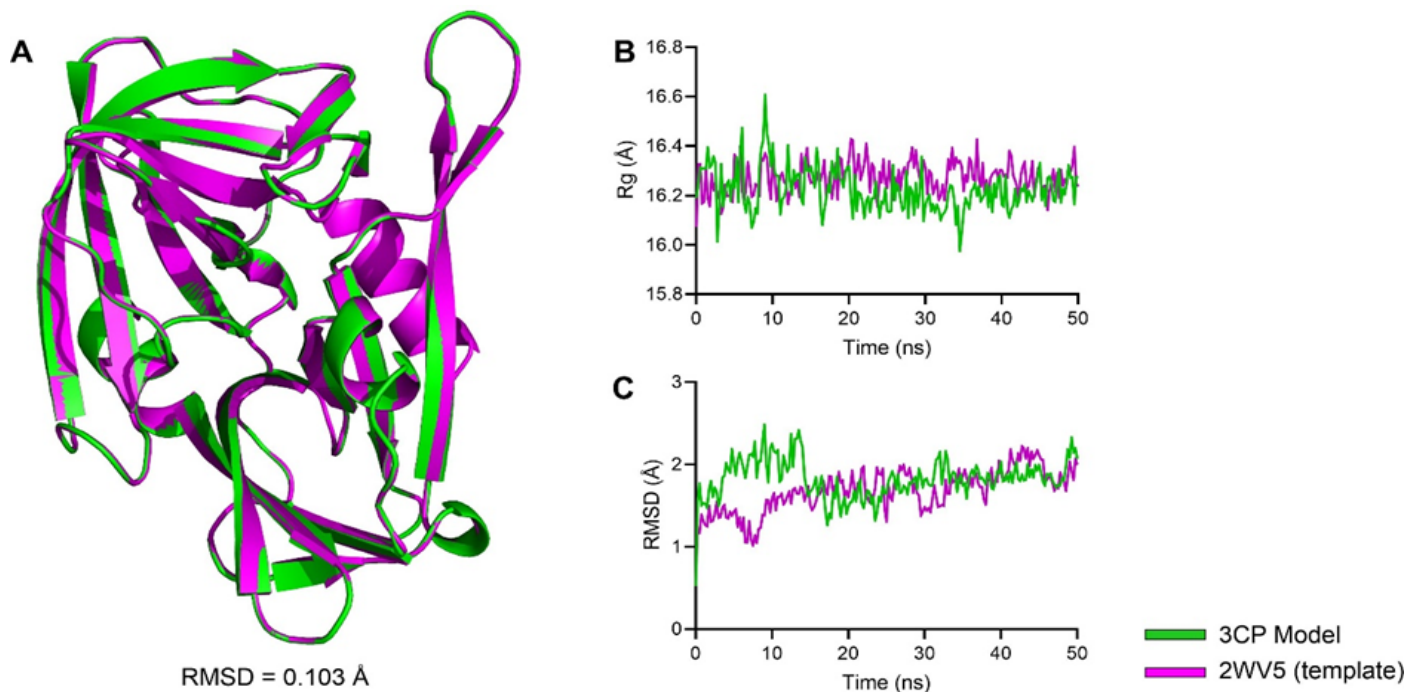


Figure 1. Structural differences and stability assessment of the 3CP of Indonesian serotypes with the template structure (PDB ID: 2WV5). Structural alignment of the model from 3CP of Indonesian serotypes (green ribbon) with the template (magenta ribbon) (A) along with the stability measures according to the Rg (B) and the RMSD of backbone atoms (C).

cated by the Radius of Gyration (Rg) and the RMSD of backbone atoms, also showed similarities between the model and the template. The Rg values revealed that both structures exhibited similar compactness, with minimal differences of less than 1 Å. Although minor fluctuations occurred during the initial 0-15 ns of the simulation, these differences were still within the range of less than 1 Å (figure 1B). The stability of the backbone atoms, as depicted in figure 1C, also demonstrated these small fluctuations. However, both structures experienced stabilization after the 15th ns of the simulation period, despite the presence of slight differences (figure 1C). Thus, small variations in the amino acid sequences of the 3CP of Indonesian serotypes have a small influence on the stability of its structure.

Electronegativity Properties

Chrysin, classified as a flavonoid based on its chemical structure, consists of two benzene rings and an additional oxygen-containing ring. It shares a similar structure with Luteolin, a compound known for its inhibitory activity against 3CP of FMDV as confirmed by Theerawatanasirikul et al. (2021). It is worth noting that Luteolin and Chrysin, two flavonoids, exhibit minor differences in their structures. These differences primarily occur in the hydroxylation patterns of the B-ring, where Luteolin possesses hydroxyl groups at positions 3' and 4', while chrysin lacks hydroxyl groups at these positions (figure 2A). Consequently, conducting a DFT analysis to evaluate their electronic properties and predict similar bioactivity against 3CP becomes an intriguing task.

The computational analysis using DFT reveals the favorable interaction potential between Chrysin and 3CP based on their respective electronegativity profiles, particularly considering the ΔE value. Notably, Chrysin exhibits a ΔE value similar to that of Luteolin, a known inhibitor of 3CP (see Figure 2B). ΔE , obtained by calculating the energy difference between the LUMO and the HOMO, reflects the molecules' capability in

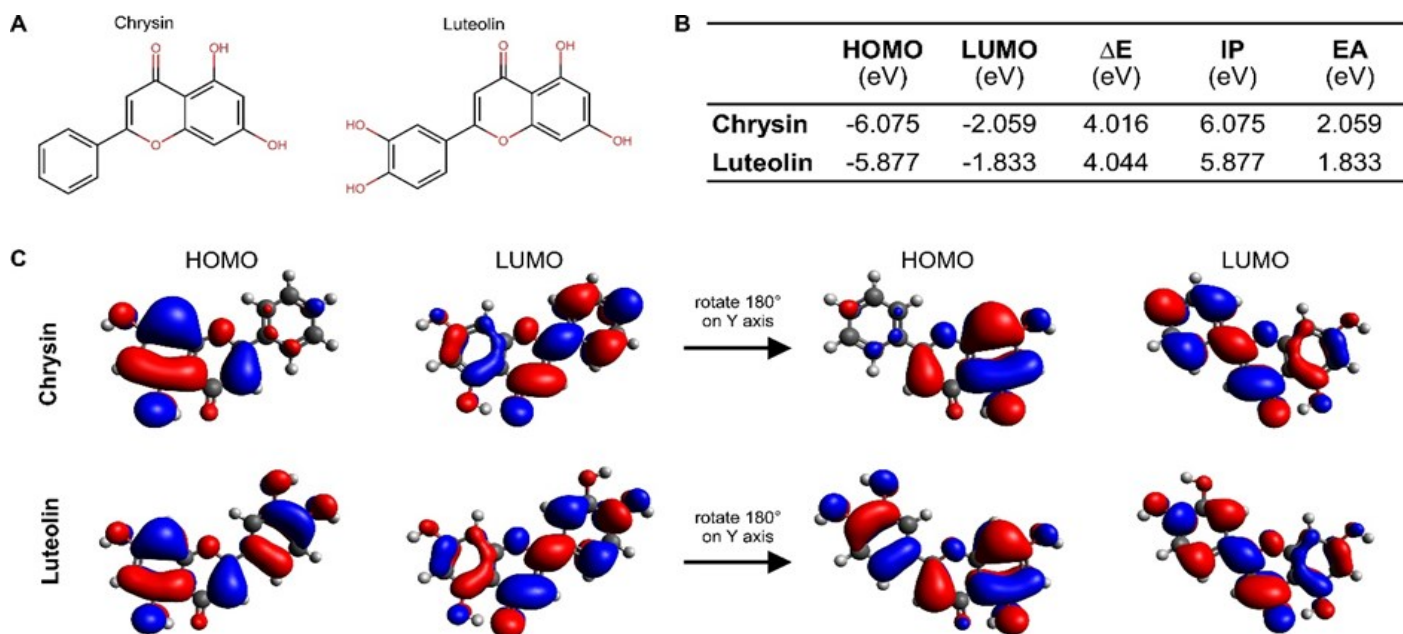


Figure 2. The structure and electronic properties of Chrysin and Luteolin. Both Chrysin and Luteolin have similar properties according to the chemical structure (A), electronegativity properties (B) and the HOMO and LUMO position (C) according to the DFT calculations.

electron transfer mechanisms (Rammohan et al. 2020). A smaller ΔE value indicates more efficient electron transfer (Islam 2015; Rammohan et al. 2020). Consequently, Chrysin is expected to have superior binding affinity towards the target protein compared to Luteolin. Furthermore, the IP and EA were determined using the Hartree-Fock (HF) model (Amati et al. 2020; Hossen et al. 2021). Molecules with lower ionization potentials and higher electron affinities possess increased reactivity and are more likely to engage in electron transfer or interaction (Rammohan et al. 2020). Hence, both Chrysin and Luteolin exhibit comparable interaction potential with Chrysin favoring an electron-donor role, while Luteolin acts as an electron acceptor during their interaction with 3CP (figure 2B).

The distribution map of HOMO and LUMO properties showed a similar pattern between Chrysin and Luteolin. Nonetheless, minor variations were observed, specifically in the B ring of both molecules (Figure 2C). Consistent with previous discussions on the impact of different functional groups on energy density (Xu et al. 2021), the presence of two hydroxyl groups appears to have an effect on the distribution of HOMO and LUMO for each molecule. Due to its hydroxyl groups, it is plausible that Luteolin possesses better activity compared to Chrysin. Despite this, based on their electronic properties, Chrysin and Luteolin are likely to interact similarly as inhibitors.

Binding of Chrysin to 3CP

As depicted in Figure 3A, the binding of Chrysin to the 3CP displayed a highly similar conformation to Luteolin. Both compounds demonstrated binding at comparable energies, although Chrysin displayed a higher binding energy than Luteolin. Notably, Chrysin and Luteolin shared a number of amino acid residues, and interactions occurred at the active site positions, specifically VAL 138, MET 141, TYR 152, and THR 156. Interestingly, Chrysin formed a greater number of hydrogen bonds during its binding to 3CP than Luteolin did. Chrysin formed hydrogen bonds with PHE 150, TYR 152, and GLY 185, whereas Luteolin bonded carbon to hydrogen with ALA 152. In addition, as shown in Figure 3B,

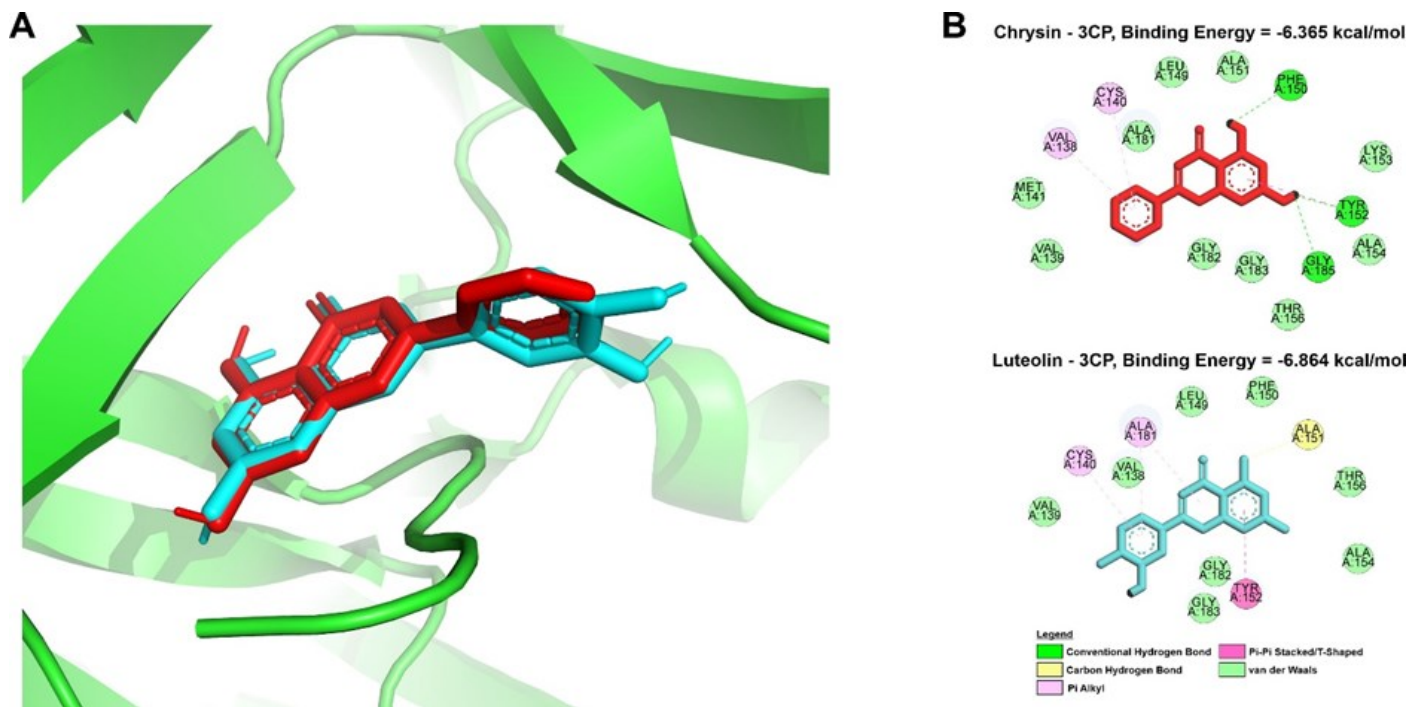


Figure 3. Structural conformation, binding energy and binding site of the Chrysin compared to the Luteolin to the 3CP. The 3D of the 3CP was visualized in green ribbon, while the Chrysin and the Luteolin were displayed in red and cyan sticks, respectively (A). Amino acids interaction was displayed in 2D map with amino acids visualized as a circular disc, and the color refers to each interaction chemistry (B).

both complexes were strengthened by hydrophobic bonds in their B- and A-rings as well as multiple Van der Waals interactions (Figure 3B). Chrysin is predicted to inhibit 3CP in a manner similar to that of Luteolin, based on the observed interaction patterns.

The 3CP enzyme plays a crucial role in the reproductive cycle of FMDV by processing the polyprotein precursor to form new viral particles (Wang et al. 2015). Previous studies have identified natural compounds capable of reducing viral load by inhibiting the 3CP, particularly for FMDV serotype A (Theerawatanasirikul et al. 2021; Theerawatanasirikul et al. 2022). One such compound is Luteolin (Theerawatanasirikul et al. 2021), which shares a similar chemical structure with Chrysin, the molecule of interest in this study. Both Chrysin and Luteolin interact effectively with key catalytic residues of the 3CP (figure 3). While Chrysin exhibits a higher binding energy than Luteolin, it forms a greater number of hydrogen bonds. As hydrogen bonds significantly contribute to the stability of protein-ligand interactions (Chen et al. 2016), Chrysin may serve as a more suitable candidate for comparison with Luteolin as an inhibitor of the 3CP. Furthermore, this study suggests that Luteolin may also exhibit similar inhibitory activity against the 3CP of FMDV serotype O, as previous investigations primarily focused on its inhibitory effects against serotype A.

Structural Dynamics of Chrysin-Bounded 3CP

The RMSD measures the deviation of an atom's position during simulations and indicates the instability of the structure (Sargsyan et al. 2017). Comparing the binding of Chrysin and Luteolin to 3CP, the RMSD of the atom backbone indicates that Chrysin-bounded 3CP is more stable (figure 4A). The Rg was also employed to evaluate the structural compactness of 3CP bound to Chrysin and Luteolin. A lower Rg value indicates greater density (Meylani et al. 2023). Until the end of the simulation, 3CP-Chrysin exhibited slightly fluctuating Rg values around 8 ns

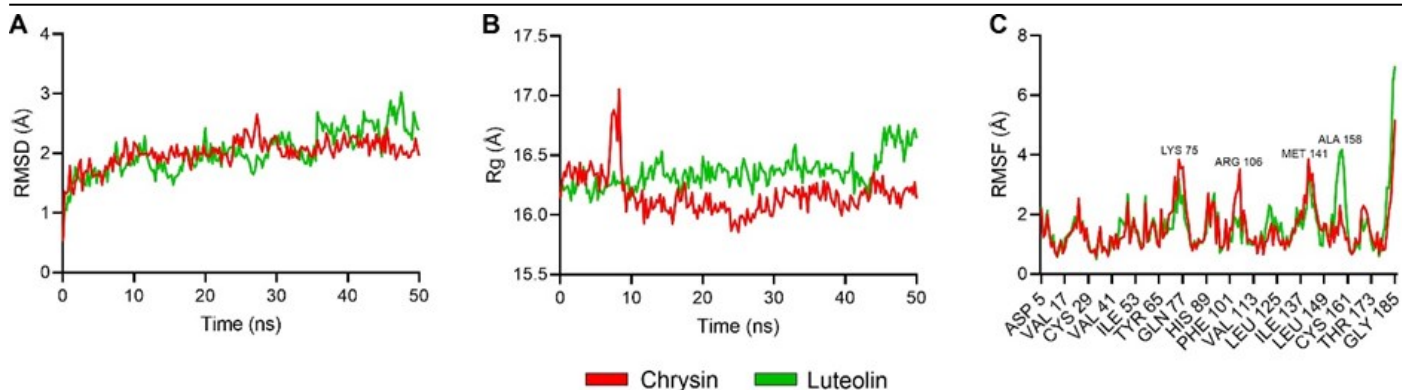


Figure 4. The structural stability of the 3CP upon binding with the Chrysin compared to the Luteolin. The structural stability was assessed through the value of the RMSD of backbone atoms (A), the radius of gyration (B), and the RMSF of each residue (C) of 3CP.

and lower Rg than 3CP-Luteolin (Figure 4B). Les disparities were negligible, less than 1 Å. The RMSF values, which indicate residual flexibility (Khan et al. 2021), differed lightly between 3CP-Chrysin and 3CP-Luteolin. Certain residues, including LYS 75, ARG 106, MET 141, ALA 158, and the C-terminal residues of 3CP, had higher RMSF values despite not being catalytic sites (Figure 4C). Only MET 141 interacted with Chrysin through Van der Waals forces. Terminal chain instability is a common characteristic of proteins (Iwakura & Honda 1996). Since ligand-induced protein conformation influences the affinity of the protein for the ligand (van den Noort et al. 2021), the degree of stabilization will minimize the dissociation of the protein-ligand complex to perform its bioactivity (Glas et al. 2017). The minimal effect of the compounds on the 3CP's structural stability, particularly Chrysin, suggests the possibility to inhibit the activity of 3CP in a stable complex formation.

From the compounds' structures and interactions point of view, Chrysin showed relatively stable conformation compared to the Luteolin. Although dramatic fluctuations appeared at around 20-30 ns, the value was less than 1 Å. A Similar event was also displayed by Luteolin, which showed some fluctuations during 7-10 ns of simulations (Figure 5A). However, Chrysin exhibited lower number of formed hydrogen bonds (Figure 5B) and described higher free-binding energy than Luteolin (Figure 5C). Previous study demonstrated that thermodynamic stability, which relates to binding affinity, does not require structural stability (Majewski et al. 2019). However, structural stability incurs an entropic penalty that hinders complex formation (Majewski et al. 2019). Hydrogen bonds contribute to this penalty, promoting a stable protein-ligand complex (Majewski et al. 2019). Hence, Chrysin may be less effective to

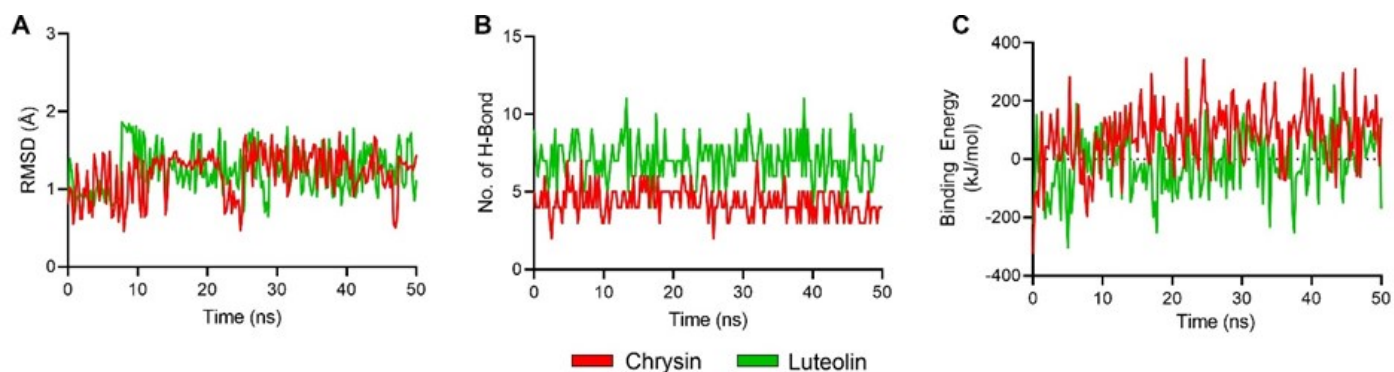


Figure 5. The stability of compounds and complexes interactions during molecular dynamics simulation. The stability of compounds as the ligands were displayed as the RMSD of ligand structure (A), while the interaction stability was assessed through the number of hydrogen bonds (B) and free-binding energy calculations (C).

interact with 3CP than Luteolin due to lower number of hydrogen bonds. Still, the differences of both compounds are plausible to perform a similar activity in inhibiting 3CP of FMDV. Nonetheless, experimental evidences are still required to validate the inhibitory properties of Chrysin against 3CP.

CONCLUSIONS

Indonesian serotype of FMDV had unique amino acid substitution at T104 and D177 compared to another O serotype. On the other hand, Chrysin has the potential as a 3CP inhibitor through its electronegativity properties, mainly at the benzene and carbonyl ring, as well as the hydroxyl group. Chrysin bound with several active sites, i.e., VAL 138, MET 141, TYR 152, and THR 156. The binding of Chrysin to 3CP remained stable without affecting the protein structure's integrity. Chrysin also showed stable structural conformation, although possessed fewer hydrogen bonds and higher free-binding energy than Luteolin. Still, Chrysin had promising potential to control FMDV infection by limiting viral replication through 3CP inhibition. Experimental validation is warranted to confirm these predictions and determine the therapeutic efficacy of Chrysin in combating FMDV infections.

AUTHOR CONTRIBUTION

AS acquired the funding and designed the experiment, MC analyzed and visualized the data, NN and DP wrote and revised the manuscript, FEH and EPP performed the experiments and calculations. All authors agreed to the final version of this manuscript.

ACKNOWLEDGMENTS

The authors thank Prof. Nashi Widodo, Ph.D.Med.Sc. for providing a license for YASARA Structure software. This research was funded by Internal Research Grant (Hibah Penelitian Unggulan) of Brawijaya University under funding scheme no. 975.37/UN10.C10/PN/2021.

CONFLICT OF INTEREST

The authors declare no conflict of interest raised in this study.

REFERENCES

- Amati, M., Stoia, S. & Baerends, E.J., 2020. The Electron Affinity as the Highest Occupied Anion Orbital Energy with a Sufficiently Accurate Approximation of the Exact Kohn–Sham Potential. *Journal of Chemical Theory and Computation*, 16(1), pp.443–452. doi: 10.1021/acs.jctc.9b00981.
- Anjum, S.I. et al., 2019. Composition and functional properties of propolis (bee glue): A review. *Saudi Journal of Biological Sciences*, 26(7), pp.1695–1703. doi: 10.1016/j.sjbs.2018.08.013.
- Bálint, D. & Jäntschi, L., 2021. Comparison of Molecular Geometry Optimization Methods Based on Molecular Descriptors. *Mathematics*, 9(22), p.2855. doi: 10.3390/math9222855.
- Carrillo, C. et al., 2005. Comparative genomics of foot-and-mouth disease virus. *Journal of Virology*, 79(10), pp.6487–6504. doi: 10.1128/JVI.79.10.6487-6504.2005.
- Chen, D. et al., 2016. Regulation of protein-ligand binding affinity by hydrogen bond pairing. *Science Advances*, 2(3), p.e1501240. doi: 10.1126/sciadv.1501240.

- Curry, S. et al., 2007. Foot-and-mouth disease virus 3C protease: Recent structural and functional insights into an antiviral target. *The International Journal of Biochemistry & Cell Biology*, 39(1), pp.1–6. doi: 10.1016/j.biocel.2006.07.006.
- Dallakyan, S. & Olson, A.J., 2015. Small-molecule library screening by docking with PyRx. *Methods in Molecular Biology (Clifton, N.J.)*, 1263, pp.243–250. doi: 10.1007/978-1-4939-2269-7_19.
- Eberhardt, J. et al., 2021. AutoDock Vina 1.2.0: New Docking Methods, Expanded Force Field, and Python Bindings. *Journal of Chemical Information and Modeling*, 61(8), pp.3891–3898. doi: 10.1021/acs.jcim.1c00203.
- Glas, A. et al., 2017. Increased Conformational Flexibility of a Macrocyclic–Receptor Complex Contributes to Reduced Dissociation Rates. *Chemistry – A European Journal*, 23(64), pp.16157–16161. doi: 10.1002/chem.201702776.
- Grubman, M.J. & Baxt, B., 2004. Foot-and-mouth disease. *Clinical Microbiology Reviews*, 17(2), pp.465–493. doi: 10.1128/CMR.17.2.465-493.2004.
- Hall, T.A., 1999. BioEdit: a user-friendly biological sequence alignment editor and analysis program for Windows 95/98/NT. *Nucleic Acids Symp. Ser.*, 41, pp.95–98.
- Han, S.-C., Guo, H.-C. & Sun, S.-Q., 2015. Three-dimensional structure of foot-and-mouth disease virus and its biological functions. *Archives of Virology*, 160(1), pp.1–16. doi: 10.1007/s00705-014-2278-x.
- Hanwell, M.D. et al., 2012. Avogadro: an advanced semantic chemical editor, visualization, and analysis platform. *Journal of Cheminformatics*, 4, 17. doi: 10.1186/1758-2946-4-17.
- Hermanto, F.E. et al., 2022. On The Hypolipidemic Activity of Elicited Soybeans: Evidences Based on Computational Analysis. *Indonesian Journal of Chemistry*, 22(6), pp.1626–1636. doi: 10.22146/ijc.75777.
- Hermanto, F.E., Rifa'i, M. & Widodo, 2019. Potential role of glyceollin as anti-metastatic agent through transforming growth factor- β receptors inhibition signaling pathways: A computational study. *AIP Conference Proceedings*, 2155, 020035. doi: 10.1063/1.5125539.
- Hidayat, S.A. et al., 2022. Optimization of East Java Propolis Extraction as Anti SARS-Cov-2 by Molecular Docking Study. *Jurnal Ilmu dan Teknologi Hasil Ternak (JITEK)*, 17(2), pp.123–134. doi: 10.21776/ub.jitek.2022.017.02.7.
- Homeyer, N. & Gohlke, H., 2012. Free Energy Calculations by the Molecular Mechanics Poisson-Boltzmann Surface Area Method. *Molecular Informatics*, 31(2), pp.114–122. doi: 10.1002/minf.201100135.
- Hossen, J., Ali, M.A. & Reza, S., 2021. Theoretical investigations on the antioxidant potential of a non-phenolic compound thymoquinone: a DFT approach. *Journal of Molecular Modeling*, 27(6), 173. doi: 10.1007/s00894-021-04795-0.
- IFRC, 2022, 'Indonesia: Foot and Mouth Disease Outbreak - Emergency Plan of Action (EPoA), DREF Operation n° MDRID024 - Indonesia' in *ReliefWeb*, Indonesia viewed October 24 2022, from International Federation of Red Cross And Red Crescent Societies. Available at: <https://reliefweb.int/report/indonesia/indonesia-foot-and-mouth-disease-outbreak-emergency-plan-action-epoa-dref-operation-ndeg-mdrid024>
- Islam, N., 2015. Investigation of comparative shielding of Morin against oxidative damage by radicals: A DFT study G. Weaver, ed. *Cogent Chemistry*, 1(1), 1078272. doi: 10.1080/23312009.2015.1078272.

- Iwakura, M. & Honda, S., 1996. Stability and reversibility of thermal denaturation are greatly improved by limiting terminal flexibility of *Escherichia coli* dihydrofolate reductase. *Journal of Biochemistry*, 119(3), pp.414–420. doi: 10.1093/oxfordjournals.jbchem.a021257.
- Kamel, M., El-Sayed, A. & Castañeda Vazquez, H., 2019. Foot-and-mouth disease vaccines: recent updates and future perspectives. *Archives of Virology*, 164(6), pp.1501–1513. doi: 10.1007/s00705-019-04216-x.
- Khan, Abbas et al., 2021. The SARS-CoV-2 B.1.618 variant slightly alters the spike RBD–ACE2 binding affinity and is an antibody escaping variant: a computational structural perspective. *RSC Advances*, 11(48), pp.30132–30147. doi: 10.1039/D1RA04694B.
- Kim, S. et al., 2023. PubChem 2023 update. *Nucleic Acids Research*, 51(D1), pp.D1373–D1380. doi: 10.1093/nar/gkac956.
- Krieger, E. & Vriend, G., 2015. New ways to boost molecular dynamics simulations. *Journal of Computational Chemistry*, 36(13), pp.996–1007. doi: 10.1002/jcc.23899.
- Li, K. et al., 2021. Virus–Host Interactions in Foot-and-Mouth Disease Virus Infection. *Frontiers in Immunology*, 12, 571509. doi: 10.3389/fimmu.2021.571509
- Maier, J.A. et al., 2015. ff14SB: Improving the Accuracy of Protein Side Chain and Backbone Parameters from ff99SB. *Journal of Chemical Theory and Computation*, 11(8), pp.3696–3713. doi: 10.1021/acs.jctc.5b00255.
- Majewski, M., Ruiz-Carmona, S. & Barril, X., 2019. An investigation of structural stability in protein-ligand complexes reveals the balance between order and disorder. *Communications Chemistry*, 2, 110. doi: 10.1038/s42004-019-0205-5.
- Maqsood, N. et al., 2022. DFT study of alkali and alkaline earth metal-doped benzocryptand with remarkable NLO properties. *RSC Advances*, 12(25), pp.16029–16045. doi: 10.1039/d2ra02209e.
- Meylani, V. et al., 2023. Molecular Docking Analysis of Cinnamomum zeylanicum Phytochemicals against Secreted Aspartyl proteinase 4–6 of *Candida albicans* as Anti-Candidiasis Oral. *Results in Chemistry*, 5, 100721. doi: 10.1016/j.rechem.2022.100721.
- Neese, F. et al., 2020. The ORCA quantum chemistry program package. *The Journal of Chemical Physics*, 152(22), 224108. doi: 10.1063/5.0004608.
- van den Noort, M., de Boer, M. & Poolman, B., 2021. Stability of Ligand-induced Protein Conformation Influences Affinity in Maltose-binding Protein. *Journal of Molecular Biology*, 433(15), 167036. doi: 10.1016/j.jmb.2021.167036.
- O’Boyle, N.M. et al., 2011. Open Babel: An open chemical toolbox. *Journal of Cheminformatics*, 3, 33. doi: 10.1186/1758-2946-3-33.
- Palko, N., Grishina, M. & Potemkin, V., 2021. Electron Density Analysis of SARS-CoV-2 RNA-Dependent RNA Polymerase Complexes. *Molecules*, 26(13), 3960. doi: 10.3390/molecules26133960.
- Ramírez-Velásquez, I. et al., 2022. Shape Theory Applied to Molecular Docking and Automatic Localization of Ligand Binding Pockets in Large Proteins. *ACS Omega*, 7(50), pp.45991–46002. doi: 10.1021/acsomega.2c02227.
- Rammohan, A. et al., 2020. In silico, in vitro antioxidant and density functional theory based structure activity relationship studies of plant polyphenolics as prominent natural antioxidants. *Arabian Journal of Chemistry*, 13(2), pp.3690–3701. doi: 10.1016/j.arabjc.2019.12.017.

- Roqué Rosell, N.R. et al., 2014. Design and synthesis of irreversible inhibitors of foot-and-mouth disease virus 3C protease. *Bioorganic & Medicinal Chemistry Letters*, 24(2), pp.490–494. doi: 10.1016/j.bmcl.2013.12.045.
- Rosyidi, D. et al., 2018. Perbandingan Sifat Antioksidan Propolis pada Dua Jenis Lebah (*Apis mellifera* dan *Trigona* sp.) di Mojokerto dan Batu, Jawa Timur, Indonesia. *Jurnal Ilmu dan Teknologi Hasil Ternak (JITEK)*, 13(2), pp.108–117. doi: 10.21776/ub.jitek.2018.013.02.5.
- Ryde, U. & Söderhjelm, P., 2016. Ligand-Binding Affinity Estimates Supported by Quantum-Mechanical Methods. *Chemical Reviews*, 116(9), pp.5520–5566. doi: 10.1021/acs.chemrev.5b00630.
- Sargsyan, K., Grauffel, C. & Lim, C., 2017. How Molecular Size Impacts RMSD Applications in Molecular Dynamics Simulations. *Journal of Chemical Theory and Computation*, 13(4), pp.1518–1524. doi: 10.1021/acs.jctc.7b00028.
- Siiskonen, A. & Priimagi, A., 2017. Benchmarking DFT methods with small basis sets for the calculation of halogen-bond strengths. *Journal of Molecular Modeling*, 23(2), 50. doi: 10.1007/s00894-017-3212-4.
- Song, J.-H. et al., 2015. Antiviral Activity of Chrysin Derivatives against Coxsackievirus B3 in vitro and in vivo. *Biomolecules & Therapeutics*, 23(5), pp.465–470. doi: 10.4062/biomolther.2015.095.
- Šuran, J. et al., 2021. Propolis Extract and Its Bioactive Compounds—From Traditional to Modern Extraction Technologies. *Molecules*, 26(10), 2930. doi: 10.3390/molecules26102930.
- Tesfaye, Y., Khan, F. & Gelaye, E., 2022. Vaccine matching and antigenic variability of foot-and-mouth disease virus serotypes O and A from 2018 Ethiopian isolates. *International Microbiology*, 25(1), pp.47–59. doi: 10.1007/s10123-021-00178-w.
- Theerawatanasirikul, S. et al., 2022. Andrographolide and Deoxyandrographolide Inhibit Protease and IFN-Antagonist Activities of Foot-and-Mouth Disease Virus 3Cpro. *Animals*, 12(15), 1995. doi: 10.3390/ani12151995.
- Theerawatanasirikul, S. et al., 2021. Natural Phytochemicals, Luteolin and Isoginkgetin, Inhibit 3C Protease and Infection of FMDV, In Silico and In Vitro. *Viruses*, 13(11), 2118. doi: 10.3390/v13112118.
- Trott, O. & Olson, A.J., 2010. AutoDock Vina: improving the speed and accuracy of docking with a new scoring function, efficient optimization and multithreading. *Journal of computational chemistry*, 31(2), pp.455–461. doi: 10.1002/jcc.21334.
- Trusheva, B. et al., 2011. Indonesian propolis: chemical composition, biological activity and botanical origin. *Natural Product Research*, 25(6), pp.606–613. doi: 10.1080/14786419.2010.488235.
- Wang, G. et al., 2015. How foot-and-mouth disease virus receptor mediates foot-and-mouth disease virus infection. *Virology Journal*, 12, 9. doi: 10.1186/s12985-015-0246-z.
- Wang, J. et al., 2014. Anti-Enterovirus 71 Effects of Chrysin and Its Phosphate Ester. *PLOS ONE*, 9(3), e89668. doi: 10.1371/journal.pone.0089668.
- Waterhouse, A. et al., 2018. SWISS-MODEL: homology modelling of protein structures and complexes. *Nucleic Acids Research*, 46(W1), pp.W296–W303. doi: 10.1093/nar/gky427.

- Weigend, F. & Ahlrichs, R., 2005. Balanced basis sets of split valence, triple zeta valence and quadruple zeta valence quality for H to Rn: Design and assessment of accuracy. *Physical Chemistry Chemical Physics*, 7(18), pp.3297–3305. doi: 10.1039/B508541A.
- Xu, Y. et al., 2021. HOMO–LUMO Gaps and Molecular Structures of Polycyclic Aromatic Hydrocarbons in Soot Formation. *Frontiers in Mechanical Engineering*, 7, 744001. doi: 10.3389/fmech.2021.744001
- Yele, V. et al., 2021. DFT calculation, molecular docking, and molecular dynamics simulation study on substituted phenylacetamide and benzohydrazide derivatives. *Journal of Molecular Modeling*, 27(12), 359. doi: 10.1007/s00894-021-04987-8.
- Zulhendri, F. et al., 2021. Antiviral, Antibacterial, Antifungal, and Antiparasitic Properties of Propolis: A Review. *Foods*, 10(6), 1360. doi: 10.3390/foods10061360.
- Zunzain, P.A. et al., 2010. Insights into cleavage specificity from the crystal structure of foot-and-mouth disease virus 3C protease complexed with a peptide substrate. *Journal of Molecular Biology*, 395(2), pp.375–389. doi: 10.1016/j.jmb.2009.10.048.

SUPPLEMENTARY FILES

Table S1. The list of the amino acid sequences of 3CP from other serotype of FMDV along with the accession code in GenBank database.

No.	Locality	GenBank ID
1.	Indonesia	AAT01756.1
2.	United Kingdom	AAT01779.1
3.	Belgium	AAT01760.1
4.	Italy	AAT01773.1
5.	Poland	AAT01769.1
6.	Iran	AAT01777.1
7.	Turkey	AAT01766.1
8.	South Korea	AAT01767.1
9.	Philippines	AAT01754.1
10.	India	AAT01771.1
11.	Taiwan	AAT01778.1
12.	Japan	BAC06475.1
13.	China	AAM33345.1
14.	South Africa	AAK97007.1
15.	South Africa	AAK97010.1
16.	South Africa	AAK97009.1
17.	India	ACJ02480.1
18.	South Africa	AAM53441.1
19.	India	AAC36727.1
20.	Argentina	AAT01712.1
21.	Argentina	AAT01710.1
22.	Uruguay	AAT01744.1
23.	Uruguay	AAT01745.1
24.	Netherland	AAT01694.1
25.	Germany	AAT01702.1
26.	Great Britain	AAT01695.1
27.	France	AAT01723.1
28.	Italy	AAT01735.1
29.	Spain	AAT01721.1
30.	Philippines	AAT01736.1
31.	Thailand	AAT01698.1
32.	Turkey	AAT01708.1
33.	Iran	AAT01708.1
34.	Iran	AAT01734.1
35.	Iraq	AAT01705.1
36.	Iraq	AAT01706.1
37.	Kenya	AAT01704.1
38.	Kenya	AAT01709.1
39.	Lebanon	AAT01742.1
40.	Lebanon	AAT01743.1
41.	Pakistan	AAT01738.1
42.	Israel	AAT01739.1
43.	China	AAQ90285.1
44.	Great Britain	AAT01753.1
45.	Switzerland	AAT01747.1
46.	Germany	AAT01748.1
47.	Brazil	AAT01749.1
48.	Brazil	AAT01750.1
49.	Argentina	AAT01751.1
50.	Argentina	AAT01752.1
51.	Botswana	AAT01788.1
52.	Zimbabwe	AAT01789.1
53.	United Kingdom	AAT01782.1

Table S1. Contd.

No.	Locality	GenBank ID
54.	Israel	AAT01787.1
55.	South Africa	AAT01785.1
56.	Namibia	AAT01786.1
57.	Kenya	AT01792.1
58.	Botswana	AAT01794.1
59.	Zimbabwe	AAQ11227.1

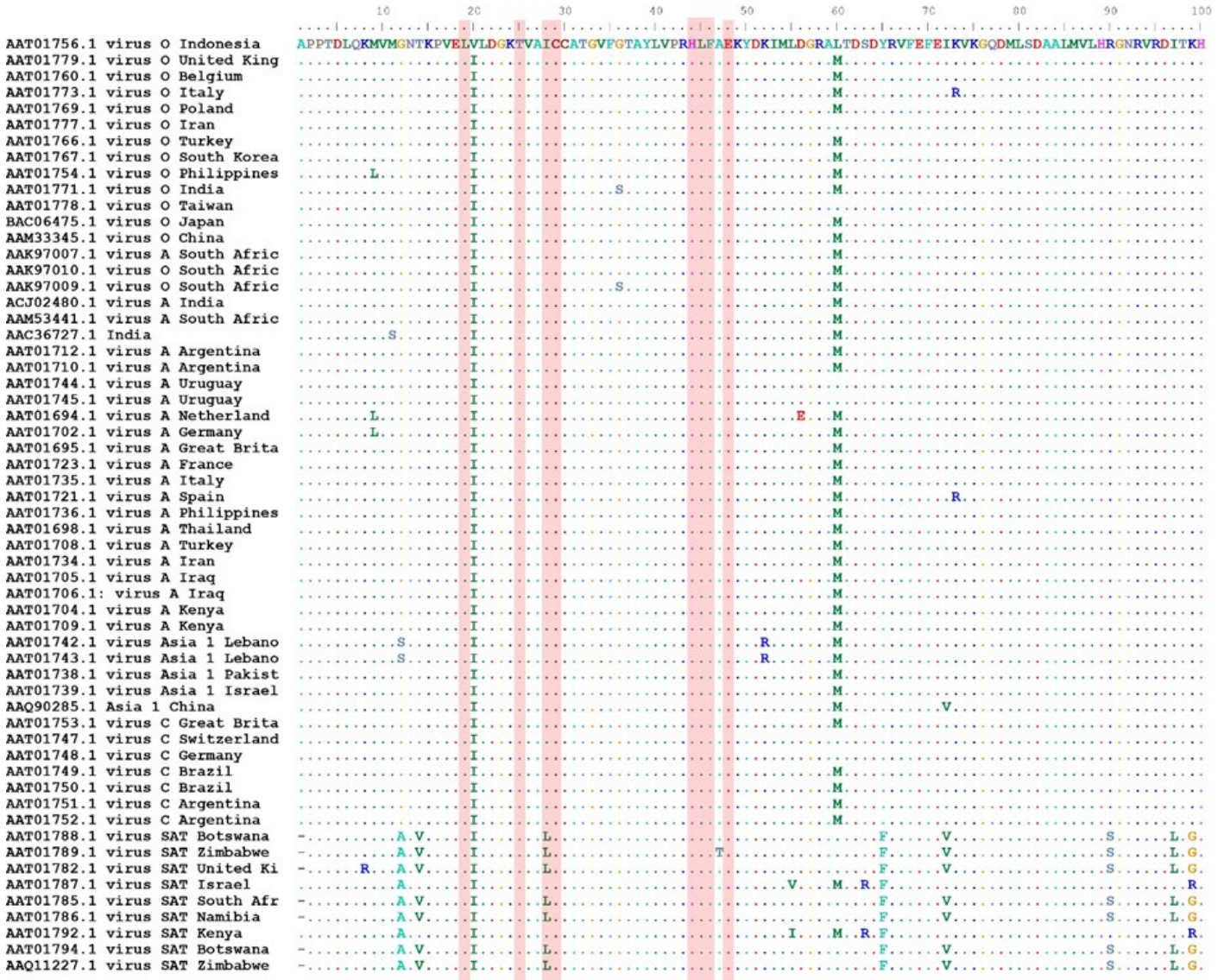


Figure S1. Multiple pairwise alignment of the 3CP sequences among several serotypes worldwide, including Indonesian serotype. The highlighted sequences indicated the active site residues.



Figure S1. Contd.